

Diamond crystals for H^- injection

U. I. Uggerhøj¹ and J. P. F. Sellschop²

¹*Department of Physics and Astronomy, University of Aarhus, DK-8000 Aarhus C, Denmark*

²*Schonland Research Institute for Nuclear Sciences, University of the Witwatersrand, P.O. WITS, 2050 Johannesburg, South Africa*

(Received 30 January 2002; published 22 July 2002)

There are several advantages in using a crystal for stripping of the H^- ion to obtain efficient injection of protons into a circular accelerator. First, the stripping efficiency of a crystal is at least as large as for an amorphous foil of the same substance and thickness. Second, the emittance increase imposed by the multiple Coulomb scattering of the protons on subsequent turns is drastically lower by a factor of up to ≈ 7 . Third, the restricted energy loss of the protons is lower by a factor of up to ≈ 1.5 —this, combined with the fact that the thermal conductivity of a single crystal of diamond is much higher than that of the amorphous material, will reduce the effect of heating of the stripping material. In high-power schemes based on amorphous foils heating of the electron stripping material is a limiting factor. Fourth, the reduced total energy loss is accompanied by a smaller energy loss straggling implying a smaller longitudinal emittance. Last, the so-called random orientation of the crystal can provide the option of stripping the H^- ions as in an amorphous foil while preserving the advantage of a high thermal conductivity, simply by changing the orientation of the crystal. A simulation using realistic parameters is presented, which reflects the efficient conservation of emittance using a diamond crystal. The phenomenon should in fact be applicable in general for the stripping of H^- , although the advantages depend on parameters such as the energy. A reasonable figure of merit is the ratio of the total transverse emittance increase of crystalline and amorphous foils in one turn and in the presented case this is as high as a factor 3.9.

DOI: 10.1103/PhysRevSTAB.5.073501

PACS numbers: 29.27.Ac, 61.85.+p, 41.85.Ar, 81.05.Uw

I. INTRODUCTION

Since the invention of phase-space filling by H^- charge-exchange injection [1] a number of different machines have employed this method to obtain intense and/or low emittance proton beams.

That the method is still widely used can be inferred from the large number of projects using such injection schemes that are being constructed or designed: the Japanese Hadron Facility, the European Spallation Source, and the Austron Spallation Source, to mention a few examples. We stress that the proposed scheme for charge-exchange injection by means of diamonds in *all* cases presents advantages compared to carbon, but the extent of the benefits depends on specific parameters such as energy, initial emittance, intensity, etc. as elaborated upon below.

Although other schemes have been proposed, e.g., field detachment of the H^- ion to H^0 followed by laser excitation and subsequent Lorentz stripping of the resulting $3P$ state of H^0 [2], the injection schemes in the above machines are all based on electron stripping in an amorphous foil.

Recent developments in the production of ultrathin single crystal diamond wafers have now raised the prospect of making large diamonds (about a cm on each side) of thicknesses as low as a μm , corresponding to about $350 \mu\text{g}/\text{cm}^2$.

We propose to use such crystals for the charge-exchange injection schemes based on stripping foils since diamond offers many advantages compared to amorphous carbon, and the only apparent drawback is the slightly more complicated mounting and control of the stripping foil.

II. CHANNELING IN CRYSTALS

The large fields present near the nuclei in solid materials may in the case of single crystals add coherently such that a penetrating particle experiences a continuous field along its direction of motion. If further the particle is incident with a sufficiently small angle to a particular crystallographic direction, inside the so-called Lindhard angle, the negatively/positively charged particle is constrained to move near/far from the nuclei and the electron clouds surrounding these; see Fig. 1. This is the channeling phenomenon [3] which has found widespread applications in physics.

The transverse potential in which the positively charged, channeled particle moves is centered away from the nuclei, while the reversed potential of a negatively charged particle is centered at the nuclei. In the case of axial channeling these nuclei constitute a string of atoms along which the particle moves. A general introduction to channeling of high energy particles and many other applications thereof can be found in [5–7].

A commonly used and rather accurate approximation to the transverse potential is the Doyle-Turner model, where

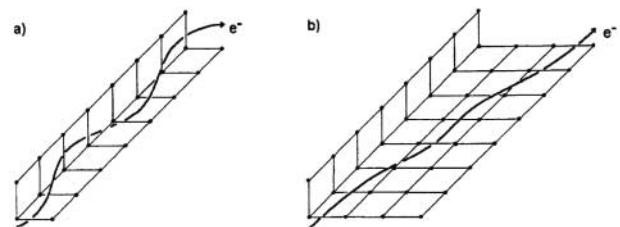


FIG. 1. A channeled negatively charged particle moves near (a) an axis, (b) a plane [4].

the thermally averaged single-string potential for a proton is given by

$$U(r_{\perp}) = \frac{2e^2 a_0}{d} \sum_{i=1}^4 \frac{a_i}{B_i + \rho^2} \exp\left(-\frac{r_{\perp}^2}{B_i + \rho^2}\right), \quad (1)$$

where r_{\perp} is the transverse distance to the string of atoms constituting the axis, $B_i = b_i/4\pi^2$, and the constants a_i and b_i are tabulated [8]. Here, a_0 , d , and ρ denote the Bohr radius, the interaxial spacing, and the thermal vibration amplitude, respectively.

In the following we will use the KEK Booster Synchrotron as a specific case, although all phenomena apply to the more general case, although with varying benefit. For the KEK Booster Synchrotron the parameters used are as given in [9].

A. Surface transmission

When the particle enters the crystal along an axial direction, it acquires a transverse potential energy depending on the transverse entry position with respect to the crystal axis. This potential energy is gained at the expense of longitudinal kinetic energy, such that the transverse kinetic energy it had outside the crystal, $p v \psi_{\text{in}}^2/2$, is conserved and adds to the potential energy to give a “transverse energy”

$$E_{\perp} = \frac{1}{2} p v \psi_{\text{in}}^2 + U(r_{\perp}^{\text{in}}) = T_{\perp} + U(r_{\perp}^{\text{in}}), \quad (2)$$

where r_{\perp}^{in} is the point of entry in transverse coordinates, i.e., perpendicular to the direction of the string, ψ_{in} is the entrance angle, and p and v are the particle momentum and velocity. The result is that positively charged particles incident close to the axis cannot channel and will behave as random particles, i.e., as if in an amorphous material. However, as the probability for this is roughly equal to the transverse area which the string occupies due to the thermal vibration amplitude, ρ , compared to the unit cell area, i.e., about $(2.5\rho)^2/r_0^2$ which is equal to a few percent [10], it contributes only marginally. Here $r_0 = 1/\sqrt{\pi N d}$ denotes the average transverse axial spacing.

On the other hand, negatively charged particles cannot channel *unless* they are near the nuclei upon entry, i.e., the probability for them to channel, the surface transmission, is exceedingly low.

B. Critical angle and oscillation wavelength

From Eq. (2) the critical angle for channeling can be derived. In the case of Lindhard’s “standard” potential [3] the result for protons along an axis is given as

$$\psi_1 = \sqrt{4Ze^2/pvd}, \quad (3)$$

where Ze is the charge of the lattice nuclei. In diamond the values at $E = 40$ MeV applicable for the KEK Booster Synchrotron [9] are $\psi_1(\langle 100 \rangle) = 1.11$ mrad, $\psi_1(\langle 110 \rangle) =$

1.32 mrad, and $\psi_1(\langle 111 \rangle) = 1.20$ mrad. For a Gaussian beam with rms divergence equal to ψ_1 the $\langle 110 \rangle$ axial surface transmission in the Doyle-Turner potential is 63%, whereas for a completely parallel beam it is 98%.

The wavelength for one channeling oscillation is roughly equal to

$$d/\psi_1 = \sqrt{4dZe^2/pv}, \quad (4)$$

which for the presented case is $0.19 \mu\text{m}$ in a $\langle 110 \rangle$ diamond such that ≈ 3 oscillations take place in a $240 \mu\text{g}/\text{cm}^2$ thick crystal. This is enough that the particle can be considered to be channeled, although studies at lower energies have shown that reaction yields from close encounter processes are not suppressed as strongly for the first 1–2 oscillations [11]. In this respect, H^- injection with single crystals performs better at low energies, where d/ψ_1 is smaller and more oscillations can take place in a crystal just thick enough to strip a substantial fraction of the incoming beam. Moreover, here we have used the thickness for the KEK amorphous foil, $240 \mu\text{g}/\text{cm}^2$, which is surely an underestimate of the optimum for a single crystal.

C. Negatively charged particles

To beneficially use a crystalline foil to strip H^- from its electrons, it is imperative that the average electron density encountered is at least as large as for an amorphous foil, preferably larger. If the particle is channeled, the redistribution of particles in the transverse directions (that is, the attraction of the negatively charged particles to the lattice nuclei) will enhance the possibility of interactions which will increase the probability of electron loss.

The loss of two electrons near a nucleus in the string will increase the transverse energy (see Fig. 2) defined in Eq. (2). This is an effect similar to the acceleration in a Tandem accelerator, only here it takes place in transverse space and increases the emittance of the beam. The transverse kinetic energy before the stripping, $T_{\perp,i}$ is preserved and added to the “flipped” potential value after the stripping. As processes like (1) are more likely than (2) due to the higher electron density, the net effect is a large increase in transverse energy as shown in Fig. 2, e.g., $T_f(i) \gg T_i(1)$.

However, as this interaction takes place only once it will be a smaller effect than the following 10–20 foil interactions for the protons [12]. Moreover, as a result of the low surface transmission for negatively charged particles, ($\epsilon_{\text{neg}} \ll \epsilon_{\text{pos}}$) and the rapid stripping which prevents channeling oscillations in the negatively charged state, it is highly unlikely that the H^- ion will channel at all. Thus the large majority of H^- ions will lose their electrons as in an amorphous material. It is thus very likely that the use of a crystal will *not* lead to an increase of emittance compared to ordinary carbon *nor* will it be a more efficient stripping material (but in any case at least as good).

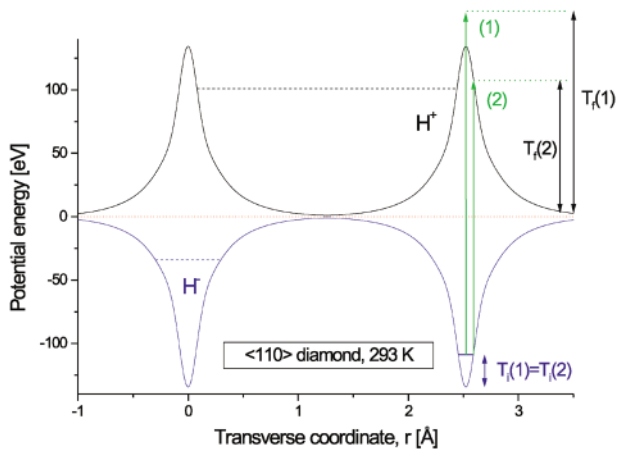


FIG. 2. (Color) The $\langle 110 \rangle$ axial potential in diamond, calculated from the Doyle-Turner model at 293 K. The upper curve represents the potential energy for protons, while the lower is for H^- . For both cases, the region accessible to a particle with $T_{\perp} = 100$ eV is shown as a horizontal dashed line. On the right, (1) and (2) denote stripping processes, where the potential “flips”; see text for details.

D. Positively charged particles

1. Multiple Coulomb scattering—transverse emittance

On subsequent turns, the protons will encounter the foil typically 10–20 times during the injection phase. Since the channeled protons are repelled from the nuclei and electrons in the crystal, the multiple Coulomb scattering is considerably reduced and the output emittance may therefore be reduced significantly. Again in this case the surface transmission is helpful since for positively charged particles, ε_{pos} is above 95% for a beam with a small rms divergence compared to ψ_1 .

In Fig. 3 is shown the normalized $\langle 100 \rangle$ electron density as a function of distance to the string, calculated from the standard model of Lindhard [3]¹ which is a simple Thomas-Fermi-type potential. Averaging along the initial direction of motion has been performed. Also shown is the allowed region of transverse coordinates, and thus electron densities encountered, for a positively charged particle with an entrance angle of half the critical angle. The average value in this case is 73% of the random value. From this it is evident that channeled protons do not encounter as many electrons as non-channeled ones, resulting in smaller multiple Coulomb scattering (MCS).

¹The $\langle 110 \rangle$ direction is a special case since the strings are connected pairwise. However the extra charge contribution from this bonding is small and can be safely neglected in this context [13].

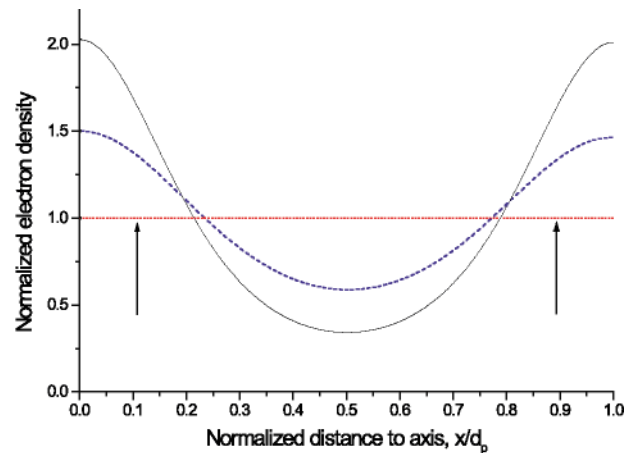


FIG. 3. (Color) The $\langle 100 \rangle$ axial electron density in diamond along the (100) (dashed line) and (110) (solid line) planes, calculated from Lindhard’s “standard” model [3], normalized to the average value shown as a dotted line. The region accessible to a particle with $\theta = \psi_1/2$ is between the arrows.

2. Restricted energy loss—temperature and longitudinal emittance

Furthermore, since protons are repelled by the lattice nuclei from regions of high electron density, the restricted energy loss and thus the heating of the crystal is also significantly reduced—up to almost a factor of 2 (see below and, e.g., [14])—with respect to incidence on a carbon foil. This means that considerations of local temperature rise are not as severely limiting and thus in this respect the lattice betatron amplitude function at the crystal can be reduced to give an even smaller emittance increase. Last, the reduced total energy loss is accompanied by a reduced energy loss straggling which means that also in the longitudinal direction the emittance increase will be smaller.

In Table I a number of parameters are given to ease the comparison between amorphous carbon and diamond.

The thermal conductivity varies according to temperature and type of diamond (type IIa as high as $15\,000\text{ W g}^{-1}\text{ K}^{-1}$ at 80 K), but in all cases it is more than about 400 times higher than for amorphous carbon.

However, possibly as important as the thermal conductivity is the emissivity since heat is mainly radiated away from the foil [15,16]. The emissivity for graphite is only ≈ 0.7 whereas for amorphous carbon (soot) it is as high as 0.96 and the number for diamond is in the neighborhood of 0.4. However, the relation between heat load, W , and temperature rise, T , is $W = \alpha_w \sigma_{SB} (T^4 - T_{\text{amb}}^4)$, where T_{amb} is the ambient temperature, σ_{SB} is the Stefan-Boltzmann constant, and α_w is the emissivity. Thus, a difference in emissivity transforms into a very small difference in temperature.

Also, the initial rate of the temperature rise is inversely proportional to the specific heat which means that the diamond will reach equilibrium slightly faster than carbon [16].

TABLE I. Comparison of parameters for a diamond and an amorphous carbon foil of the same thickness, $240 \mu\text{g}/\text{cm}^2$, penetrated by protons of an energy of 40 MeV. The values denoted by an * are taken for a transverse energy corresponding to the angular divergence, including surface transmission.

	Diamond	Carbon	Ratio
Thermal conductivity (@ 293 K)	600–1000 $\text{Wg}^{-1} \text{K}^{-1}$	1.59 $\text{Wg}^{-1} \text{K}^{-1}$	377–629
Specific heat	0.124 $\text{cal}^{-1} \text{K}^{-1}$	0.170 $\text{cal}^{-1} \text{K}^{-1}$	0.7
Emissivity	≈ 0.4	0.96	≈ 0.4
Energy loss*	2.4 keV	3.3 keV	0.72
Density	3.53	2.2	1.6
Multiple Coulomb scattering*	149 μrad	227 μrad	0.66
Radiation length, X_0	12.2 cm	18.8 cm	0.65

E. Radiation damage

The resilience of the crystalline structure to a high-power, high energy beam is evidently very important. However, experiments with bent crystals at high energy have shown that for silicon the lattice is not severely damaged until the integrated fluence exceeds values of the order of 10^{20}cm^{-2} [17]. This corresponds to only a few days of operation in most cases considered for spallation neutron sources. However, diamond undoubtedly exceeds silicon significantly in radiation hardness because the lattice is so dense that—loosely speaking—the displaced atoms will be forced back into their correct sites. Recent tests at the Stanford Linear Collider have shown that contrary to aluminum which evaporates, diamond suffers *no* visible damage when subjected to the SLAC Final Focus Test Beam, an electron beam of duration 1 ps, transverse size about $0.06 \mu\text{m}^2$, and nominally 2×10^{10} electrons per pulse at a repetition rate of 120 Hz [18], i.e., about 4×10^{21} electrons/ cm^2 per second. So radiation damage is very unlikely to pose a threat to the application.

Moreover, the heat load may actually be beneficial since the crystal lattice may rearrange itself after damage due to thermal annealing as long as the temperature stays below about 1200° . This temperature limit is within reach as the restricted energy loss, and thus the heating, is reduced to almost half, and finite-element analysis of carbon foils indicates temperatures around 1700 K [15].

III. ACCELERATOR PARAMETERS

A. Twiss parameters

The beam divergence, $\theta = \sqrt{\epsilon\gamma_T}$, at the location of the stripping crystal should be smaller than or at least comparable to ψ_1 . Here, α_T , β_T , and γ_T denote the Twiss parameters of the accelerator lattice. In the case of KEK, the divergence is smaller than the critical angle, $\theta/\psi_1 \approx 0.6$, so a significant fraction, 87%, of the beam will fulfill the channeling criterion.

Given β_T , and the emittance, ϵ , there is also a limit on the minimum size of the crystal, $\propto \sqrt{\beta_T \epsilon}$. All other things equal, since θ and ψ_1 are both proportional to $1/\sqrt{\beta\gamma}$, the

energy dependence affects only the minimum size required for the crystal.

B. Space charge

In many high-power applications it is a design aim to fill the large-emittance transverse phase space of the synchrotron with the small-emittance beam from the linac in such a way that the tune shift imposed by the space charge remains acceptable. This is done by “painting” the phase space by successive (or even correlated) vertical and horizontal bumps. In some schemes the resultant angles of incidence during painting are such that the channeling criterion cannot be fulfilled at all settings. However, we emphasize that the crystalline material never performs poorer than the amorphous material, i.e., there is always some degree of benefit. Thus, the proposed scheme is expected to be in principle generally applicable, although the advantages are variable, e.g., diminishing with increasing energy [19]. Thus, we anticipate the use in specific cases, notably for intermediate energies from a few tens to a few hundreds of MeV, where the method is most beneficial.

As an estimate of the influence of space-charge effects the tune shift is calculated from [20]

$$\Delta\nu \approx \frac{r_p N_p}{\pi \beta^2 \gamma^3 \epsilon} \quad (5)$$

in the individual particle limit, where bunching and form factors have been set to 1, $r_p = e^2/m_p c^2$ is the classical proton radius, N_p is the number of protons, and $\epsilon = \epsilon_x = \epsilon_y$ is the emittance. Then the resulting emittance increase may be estimated from [21]

$$\Delta\epsilon \approx \left\{ \left[1 + \frac{1}{2} \left(\frac{\nu_0^2}{\nu^2} - 1 \right) U \right]^{1/2} - 1 \right\} \epsilon, \quad (6)$$

which applies for a constantly focused, round beam where $U = (W - W_u)/\omega_0$ is the normalized nonlinear field energy and $\nu_0 = \nu + \Delta\nu$ with ν_0 the tune in absence of space charge. For a Gaussian beam U is set to 0.154 [21] which leads to

$$\Delta\epsilon \approx \frac{U r_p N_p}{2\nu \pi \beta^2 \gamma^3} \quad (7)$$

expressing the estimated emittance growth as a function of the number of protons and tune, given the approximations above. From this one can assess the influence of the effect of space charge on a potential application, i.e., how large a fraction of the particles is propelled to so large an emittance that they can no longer fulfil the criterion of channeling. In the presented case, the increase of the angle of incidence compared to its value in the absence of space charge is only a few percent, even for a relatively intense beam, $N_p = 1 \times 10^{12}$.

C. Nuclear activation

An important concern to the operation of the stripping section is the nuclear activation of components along the beam line due to loss of protons. The suppression of close encounter processes at high energies is given by

$$\chi_{\min} = 18.8Nd\rho^2 \quad (8)$$

in the ideal case [11]. Thus the yields of, e.g., Rutherford-backscattered protons are suppressed by large factors ($\gg 10$) for an aligned crystal compared to the random orientation. It is therefore possible to align the crystal by detecting the number of these interactions as a function of angle. Clearly, as the direct interaction is strongly reduced, the close encounter processes leading to large scattering angles are extremely infrequent *and* as the emittance increase is strongly suppressed, the nuclear activation will also be significantly reduced. This is an important aspect of the use of diamond as a replacement for carbon as it reduces the constraints on intensity due to nuclear activation of components downstream of the stripping agent.

IV. EQUIPMENT REQUIREMENTS

The crystal must be mounted such that at least one side—the one facing the beam—is unsupported. Moreover, to avoid internal stress due to the mounting of such a thin crystal, it is desirable that it be held at one point only, though with good thermal contact to a heat reservoir to limit the effect of heating. This is possible with a crystal thickness larger than a few μm . A suitable configuration would be to leave a much thicker surround of the same diamond, on at least three sides of the target crystal foil.

The orientation and position must be remotely controlled by means of a goniometer with at least 2 angular degrees of freedom (normally referred to as tilt and turn) and a displacement which does not affect the orientation. The minimum step size for the angular variables must be at least a factor of 2 smaller than the planar critical angle, $\psi_p \approx \psi_1/3$, and the displacement must have a minimum step size of 1 mm. A similar device is being used for the crystal which transports part of the proton beam used for the NA48 experiment at CERN [22].

V. SIMULATIONS

A. Amorphous material

Simulations of the survival probability, emittance increase, and thus overall efficiency have been performed following the scheme of Kawakubo [9].

The outline of these simulations is as follows: The x coordinate of the center of the betatron motion at the n th turn is given as

$$X_n = x_p \frac{\Delta p_0}{p} + \Delta x - x_p \frac{\Delta p}{p} \sum_{i=0}^{n-1} \eta_i, \quad (9)$$

where x_p is the horizontal momentum coordinate, Δp_0 is the momentum mismatching of the incident H⁻ ion, p is the momentum, Δx is the closed orbit distortion, and Δp is the ionization momentum loss found from

$$\frac{dp}{dx} = \frac{4\pi e^4 N Z_2}{m v^3} L, \quad (10)$$

where L is given by

$$L = \ln\left(\frac{2\gamma^2 m v^2}{I}\right) - \frac{C}{Z_2} - \beta^2 - \frac{\delta}{2}, \quad (11)$$

with the density effect $\delta = 2 \ln(\hbar \omega_p \beta \gamma / I) - 1$, $\omega_p = \sqrt{4\pi e^2 N Z_2 / m}$ being the plasma frequency, $I \approx Z_2 \times 10$ eV is the ionization potential, and C is the shell correction which can be safely neglected at high energies.

The probability that the particle hits the foil on the n th turn, η_n , is calculated from the phase-space geometry as

$$\eta_n = \begin{cases} 1 & (X_n - x_F \geq r_n \sqrt{\beta_T}), \\ 1 - \frac{1}{\pi} \cos^{-1}\left(\frac{X_n - x_F}{r_n \sqrt{\beta_T}}\right) & (-r_n \sqrt{\beta_T} < X_n - x_F < r_n \sqrt{\beta_T}), \\ 0 & (X_n - x_F \leq -r_n \sqrt{\beta_T}), \end{cases} \quad (12)$$

where x_F is the position of the stripping foil edge, β_T is one of the three Twiss parameters, $\alpha_T, \beta_T, \gamma_T$, and $\eta_1 \equiv 1$. Then the expected value of the square of the betatron amplitude in $(x/\sqrt{\beta_T}, \alpha x/\sqrt{\beta_T} + \sqrt{\beta_T} x')$ phase space can be calculated from

$$r_n^2 = r_0^2 + \left[\beta_T \sigma^2 + \epsilon_p \left(\frac{\Delta p}{p} \right)^2 \right] \sum_{i=1}^n \eta_i^2, \quad (13)$$

where $\epsilon_p = \gamma_T x_p^2 + 2\alpha_T x_p x_p' + \beta_T x_p'^2$ and σ denotes the rms value of the multiple Coulomb scattering

$$\sigma = \frac{13.6 \text{ MeV}}{\beta c p} \sqrt{\frac{x}{X_0}} \left[1 + 0.038 \ln\left(\frac{x}{X_0}\right) \right], \quad (14)$$

with x/X_0 as the thickness of the foil in units of the radiation length.

Finally, the survival probability on the n th turn, $\alpha_n(r_x)$, can be found from

$$\alpha_n(r_x) = 2\pi \int_0^{r_x'} P_n(r) r dr, \quad (15)$$

where

$$r_x' = r_x + \frac{x_p}{\sqrt{\beta_T}} \frac{\Delta p}{p} \sum_{i=0}^{n-1} \eta_i, \quad (16)$$

with r_x denoting the position of the scraper edge and $P_n(r)$ is given as

$$P_n(r) = \frac{1}{2\pi\sigma_n^2} I_0\left(\frac{rR_n}{\sigma_n^2}\right) \exp\left(-\frac{r^2 + R_n^2}{2\sigma_n^2}\right), \quad (17)$$

with R_n being the betatron amplitude without multiple Coulomb scattering and the accumulated multiple Coulomb scattering results in

$$\sigma_n^2 = \frac{\sigma^2 \beta_T}{2} \sum_{i=1}^n \eta_i^2 + \sigma_0^2. \quad (18)$$

Here I_0 is the first modified Bessel function and σ_0 represents the injected beam size.

For details on the procedure and definitions, see Ref. [9].

Agreement with the results obtained in [9] for the KEK H^- injection was confirmed and these results were extended, introducing the channeling concepts discussed.

B. Crystalline material

For a crystalline material, Eqs. (10) and (14) are modified as described in the following. These modifications, in turn, affect the hitting probability, the beam size, and the survival probability through the connections in the above equations.

1. Energy loss

For a relativistic particle, the energy loss of a channeled particle, $dE/dx(\bar{b})$, is given approximately by Lindhard's expression

$$\frac{dE}{dx}(\bar{b}) = \frac{Z + Z(\bar{b})}{2Z} \left(\frac{dE}{dx} \right)_{\text{random}}, \quad (19)$$

where \bar{b} denotes the transverse position of the particle with respect to the axis, $Z(\bar{b})$ is the electron density at this position, and the amorphous value, $(dE/dx)_{\text{random}}$, is found from Eq. (14).

A more elaborate calculation can be found in [23,24] where the crystal structure is properly taken into account by use of a correction term $C(\bar{b})$ which depends on the electronic charge density. In the limit $C(\bar{b}) = 0$, the more

accurate result reduces to Eq. (19) which tends to overestimate the energy loss by about 20%–30% for the best channeled particles.

As a somewhat crude estimate, Eq. (19) with $Z(\bar{b})$ taken as the lowest value in transverse space (i.e., the minimum in the full drawn curve in Fig. 3) is used to describe the average energy loss of all the channeled particles. This is done, expecting that the overestimation of the energy loss of the best channeled particles in Eq. (19) is compensated by the average particle having a higher $Z(\bar{b})$ than the best channeled state. This is clearly an approximation, but for a divergence of the order of ψ_1 or smaller, it is believed to be quite good. In any case, the aim here is not to simulate the exact behavior, but rather to show the advantages connected to using a single crystal.

The energy loss of the average channeled particle, $\overline{\Delta E_{\text{chan}}}$, is thus given by $x(Z + Z_{\text{min}})/2Z(dE/dx)_{\text{random}}$, where Z_{min} is the minimum of $Z(\bar{b})$. With sufficient accuracy we set $\overline{\Delta E_{\text{chan}}} = (dE/dx)_{\text{random}} 0.65x$ since $Z(\bar{b}) \approx 0.3Z$, as seen in Fig. 3.

2. Energy loss straggling

The mean square value of the energy loss distribution, the energy loss straggling, is given for a thick target by the Bohr expression [25]

$$\Omega^2 = 4\pi e^4 Z_2 N x \quad (20)$$

for a proton, i.e., it is proportional to the number of electrons encountered. In terms of the energy loss, this becomes

$$\Omega^2 = \frac{mv^2}{L} \Delta E, \quad (21)$$

so the straggling follows the reduction in energy loss for channeled particles. This implies that the longitudinal phase space becomes less diluted when passing a crystal compared to the passage of an amorphous material. For thin targets, the Landau distribution applies and in this case the large momentum transfers become significant leading to a distribution skewed towards high energies; for details, see, e.g., [24].

3. Multiple Coulomb scattering—dechanneling

In [26] the average dechanneling rate for axially channeled particles is derived as a sum of an electronic term, $(dE_{\perp}/dz)_e$, and a nuclear term, $(dE_{\perp}/dz)_n$, which is temperature dependent (although very little for a diamond crystal since the Debye temperature is 1860°), $(dE_{\perp}/dz) = (dE_{\perp}/dz)_e + (dE_{\perp}/dz)_n$:

$$\left(\frac{dE_{\perp}}{dz} \right)_n = \frac{E\psi_1^2}{2} \frac{1}{2z_n} \left(\frac{\exp(\epsilon_{\perp} + \epsilon_{\perp 0})}{2} + \frac{1}{3} \right) \times [1 - \exp(-(\epsilon_{\perp} + \epsilon_{\perp 0}))]^3, \quad (22)$$

and

$$\left(\frac{dE_{\perp}}{dz}\right)_e = \frac{E\psi_1^2}{2} \frac{1}{z_e} \left\{ 1 - \exp(-(\epsilon_{\perp} + \epsilon_{\perp 0})) \left[1 + \frac{1}{L_e} \ln\left(\frac{1}{1 - \exp(-(\epsilon_{\perp} + \epsilon_{\perp 0}))}\right) \right] \right\}, \quad (23)$$

where the two lengths z_e and z_n are given as

$$E/(\pi e^2 L_e N d) = 0.030 \text{ mm}, \quad (24)$$

and

$$(Ca_{TF})^2/(2\rho^2 \pi N d^2 \psi_1^2) = 0.78 \text{ mm}, \quad (25)$$

with quoted values for a beam of 40 MeV.

These lengths can be considered as dechanneling lengths for their respective processes, since for particles with transverse energies $E_{\perp B}$ and $0.3E_{\perp B}$, z_e and z_n are the lengths required to gain $E\psi_1^2/2$ in transverse energy. Here, $E_{\perp B} = Z_1 Z_2 e^2/d \ln[1 + 2(Ca_{TF}/\rho)^2]$ is the height of the potential barrier.

The logarithmic term from Bethe's stopping formula is slightly modified, $L_e = \ln(2^{3/2} m v^2/I) - 1$ and the two reduced transverse energies, $\epsilon_{\perp 0} = (Ca_{TF})^2/r_0^2$ and $\epsilon_{\perp} = 2E_{\perp}/(E\psi_1^2)$, where $\pi r_0^2 = 1/(Nd)$, are used. Here, $C \simeq \sqrt{3}$ denotes a constant introduced by Lindhard and $a_{TF} = 0.8853a_0(1 + Z^{2/3})^{-1/2}$ the Thomas-Fermi screening length.

The authors find in [27] that the expected transition to the amorphous value of dE_{\perp}/dz does not occur until E_{\perp} is above the barrier, $E_{\perp B}$. This is in [27] remedied by

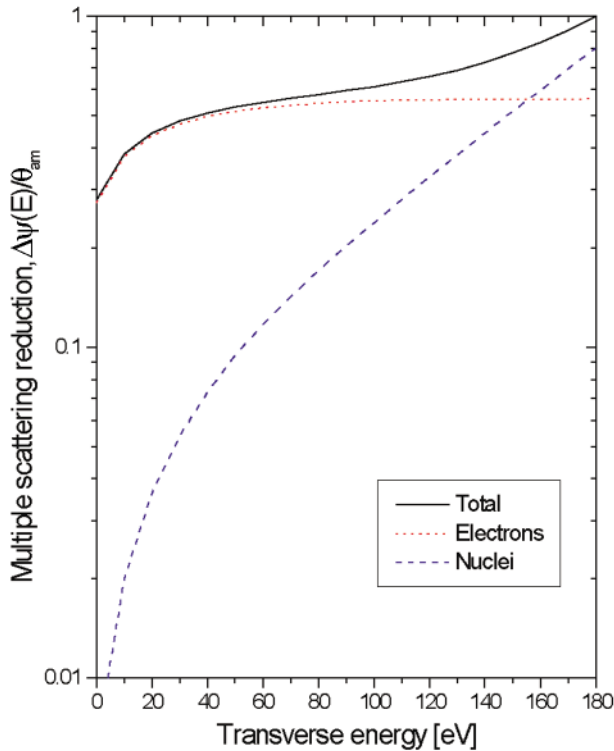


FIG. 4. (Color) The reduction factor in multiple Coulomb scattering angle, $\Delta\psi(E_{\perp B})/\sigma$, for channeled particles as a function of transverse energy based on the $\langle 110 \rangle$ axial potential in diamond.

introducing a semiempirical factor for the nuclear density at large distances from the string and modifying the electron density slightly. In the present approach we simply require $\Delta\psi(E_{\perp B}) \equiv \sigma$ and normalize (a 20% correction only) which is accurate to sufficient precision. In Fig. 4 is shown the resulting reduction factor in multiple scattering angle, $\Delta\psi(E_{\perp B})/\sigma$, as a function of transverse energy. Clearly, for high transverse energies the approximation fails, but this is not the region of main interest here. We note a drastic reduction in the nuclear contribution for small transverse energies as expected.

The average scattering angle is then found from Eq. (2) as

$$\Delta\psi(E_{\perp}) = \sqrt{2 \frac{dE_{\perp}}{dz}(E_{\perp}) x \gamma M \beta^2} \frac{\sigma}{\Delta\psi(E_{\perp B})}, \quad (26)$$

which compared to the amorphous value, Eq. (14), is about 60% such that the total transverse emittance increase is reduced by up to a factor of 7.

VI. RESULTING BEAM PARAMETERS

By means of the above formulas for the simulation and the appropriate modifications for channeled particles, we have derived the gain in using a diamond as a replacement for a carbon foil with the KEK Booster Synchrotron [9] as a specific example.

Figure 5 shows the beam size as a result of accumulated multiple Coulomb scattering, Eq. (18), as a function of the number of turns in the machine. We note that for the KEK case, the horizontal beam size after 500 turns is reduced by a factor of 1.3 by the use of a diamond crystal instead of a carbon foil. Moreover, the *increase* of the beam size is reduced by as much as a factor of 2.4 in *one* transverse direction only.

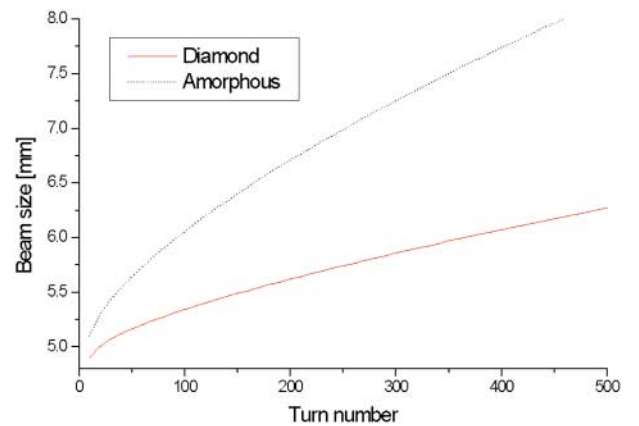


FIG. 5. (Color) The beam size at the position of the stripper foil as a function of the number of turns in the machine. The solid line is for a diamond, while the dotted line is for an amorphous carbon target, both of $240 \mu\text{g}/\text{cm}^2$.

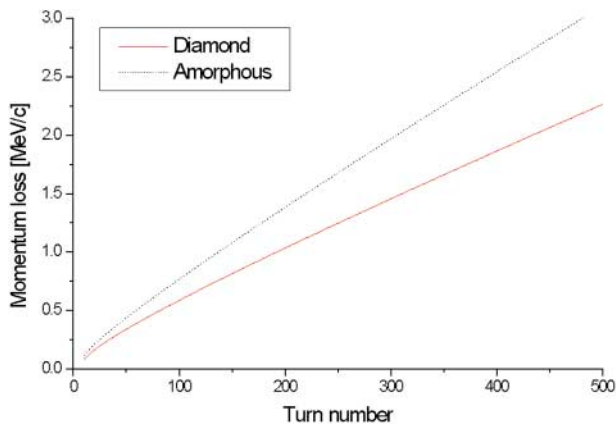


FIG. 6. (Color) The accumulated momentum loss as a function of the number of turns in the machine. The solid line is for a diamond, while the dotted line is for an amorphous carbon target, both of $240 \mu\text{g}/\text{cm}^2$.

In Fig. 6 is shown the accumulated momentum loss (proportional to the heating) as a function of the number of turns and again the diamond performs much better than the carbon foil. This, combined with the superior thermal conductivity, may alone make the crystal solution better than the amorphous foil for high-power schemes.

Figure 7 shows the survival probability, Eq. (15), as a function of the number of turns in the machine and it is seen that for the case of diamond, the injection may proceed much longer than for carbon.

The reason for this difference is obvious from Fig. 8 where the beam density, $rP_n(r)$, at turn 250 in the machine is shown. Because of the reduced momentum loss and thus smaller movement in a dispersive region *and* the reduced beam size, the beam injected through a crystal does not approach the scraper as quickly. Thus injection may proceed longer without detrimental particle loss.

However, the above figures include the injected beam size and to fully appreciate the benefits of a crystal we

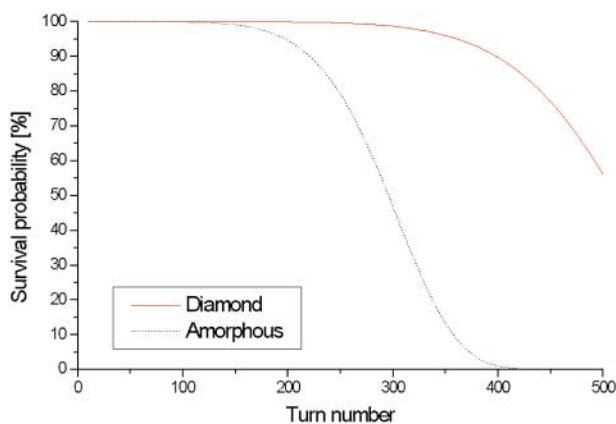


FIG. 7. (Color) The survival probability, Eq. (15), as a function of the number of turns in the machine. The solid line is for a diamond, while the dotted line is for an amorphous carbon target, both of $240 \mu\text{g}/\text{cm}^2$.

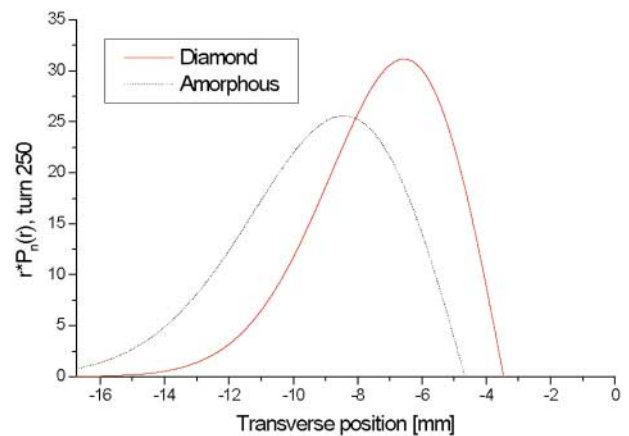


FIG. 8. (Color) The beam density, $rP_n(r)$, as a function of the horizontal position at turn 250. The solid line is for a diamond, while the dotted line is for an amorphous carbon target, both of $240 \mu\text{g}/\text{cm}^2$. The scraper is at -16.7 mm .

define a more reasonable figure of merit, $\xi = \Delta\epsilon_{\text{am}}/\Delta\epsilon_{\text{cr}}$, where $\Delta\epsilon_{\text{am}}$ is the total transverse emittance increase for an amorphous foil and $\Delta\epsilon_{\text{cr}}$ is for the crystal. For both cases we use $\Delta\epsilon = \beta\sigma^2 \sum_{i=0}^n \eta_i^2$ as the connection between the accumulated MCS angle and total emittance increase. In the considered configuration ξ is as high as 3.86 for the first turn, even when the transverse energy is calculated from the nominal angular divergence, $\theta = \sqrt{\epsilon\gamma T}$. We note that ξ^2 would be the suppression factor of the luminosity increase in a proton-proton collider based alone on the proposed injection scheme.

At this point it is worth mentioning that although the presented case is believed to be a realistic representation of a diamond replacing the carbon foil in the KEK machine as given in [9], properties such as variable closed orbit bumps to introduce phase-space painting instead of just “drift” due to momentum loss and MCS have not been included. This means that the number of interactions with the stripping foil is unrealistically high for an actual application. Nevertheless, $\xi = 3.86$ on *only one* turn remains a valid figure of merit for an evaluation of the many benefits of a diamond as a material for charge-exchange injection.

VII. CONCLUSION

We have shown examples of the many advantages offered by the use of a diamond crystal instead of an amorphous carbon foil as a stripping device for H^- injection. In order to calculate the size of the effect more accurately, a full-fledged simulation could be done where each H^- and proton is followed through the accelerator and crystal lattice. However, given the complexity of such a simulation and the fact that many parameters are still unknown, it seems more fruitful to verify the phenomenon experimentally. Such a test will be undertaken at the ASTRID accelerator at ISA, Aarhus, Denmark in the near future, using a beam of H^- ions of several tens of MeV.

ACKNOWLEDGMENT

Discussions with Horst Schönauer, Michel Martini, Massimo Giovannozzi, and Jean-Yves Hemery at CERN on the feasibility and various interactions are acknowledged. Furthermore we are grateful to S.P. Møller at ISA, Denmark, for his valuable suggestions. U.I.U. acknowledges “Steno” Grant No. 51-00-0568 from the Danish Natural Science Research Council. J.P.F.S. records with appreciation the provision of materials for research purposes by Messrs. De Beers Industrial Diamonds (Pty) Ltd.

-
- [1] G. I. Budker and G. I. Dimov, in *Proceedings of the International Conference on High Energy Accelerators, Dubna, 1963* (U.S. Atomic Energy Commission, Oak Ridge, 1963), p. 1372.
- [2] I. Yamane, *Phys. Rev. ST Accel. Beams* **1**, 053501 (1998).
- [3] J. Lindhard, *Mat. Fys. Medd. K. Dan. Vidensk. Selsk.* **34**, 1 (1965).
- [4] P.M. Weinmann, Ph.D. thesis, Technischen Universität München, 1998 (Report No. MPI-PhE/98-07).
- [5] A. H. Sørensen and E. Uggerhøj, *Nucl. Sci. Appl.* **3**, 147 (1989).
- [6] U. Mikkelsen, Ph.D. thesis, Aarhus University, 1997 (Report No. CERN-THESIS-97-009).
- [7] S.P. Møller, *Nucl. Instrum. Methods Phys. Res., Sect. A* **361**, 403 (1995).
- [8] P. A. Doyle and P. S. Turner, *Acta Crystallogr. Sect. A* **24**, 390 (1968).
- [9] T. Kawakubo, *Nucl. Instrum. Methods Phys. Res., Sect. A* **265**, 351 (1988).
- [10] J. U. Andersen, *Nucl. Instrum. Methods* **170**, 1 (1980); J. U. Andersen, E. Bonderup, E. Lægsgård, B. B. Marsh, and A. H. Sørensen, *Nucl. Instrum. Methods Phys. Res.* **194**, 209 (1982).
- [11] D. S. Gemmell, *Rev. Mod. Phys.* **46**, 129 (1974).
- [12] J. Beebe-Wang, Y. Y. Lee, D. Raparia, J. Wei, C. R. Prior, and S. Mashida, in *Proceedings of the European Particle Accelerator Conference, Vienna, 2000* (European Phys. Society, Geneva, 2000), p. 1465.
- [13] J. U. Andersen (private communication).
- [14] S. Pape Møller, V. Biryukov, S. Datz, P. Grafström, H. Knudsen, H. F. Krause, C. Scheidenberger, U. I. Uggerhøj, and C. R. Vane, *Phys. Rev. A* **64**, 032902 (2001).
- [15] C. J. Liaw, Y. Y. Lee, J. Alessi, and J. Tuozzolo, in *Proceedings of the Particle Accelerator Conference, New York, 1999* (IEEE, Piscataway, NJ, 1999), p. 3300.
- [16] J. Duke, in *Proceedings of the 5th European Particle Accelerator Conference, Barcelona, Spain, 1996* (Institute of Physics, Bristol, U.K., 1996), p. 2465.
- [17] C. Biino *et al.*, *Phys. Lett. B* **403**, 163 (1997).
- [18] P. Krejcik (private communication).
- [19] U. I. Uggerhøj, S. P. Møller, and J. P. F. Sellschop, in *Proceedings of the European Particle Accelerator Conference, Paris, 2002* (to be published).
- [20] C. Bovet, R. Gouiran, I. Gumowski, and K. H. Reich, Report No. CERN/MPS-SI/Int. DL/70/4, 1970 (unpublished).
- [21] I. Hofmann and J. Struckmeier, *Part. Accel.* **21**, 69 (1987).
- [22] N. Doble, L. Gatignon, and P. Grafström, *Nucl. Instrum. Methods Phys. Res., Sect. B* **119**, 181 (1996).
- [23] H. Esbensen and J. A. Golovchenko, *Nucl. Phys.* **A298**, 382 (1978).
- [24] H. Esbensen *et al.*, *Phys. Rev. B* **18**, 1039 (1978).
- [25] N. Bohr, *Philos. Mag.* **30**, 581 (1915).
- [26] E. Bonderup, H. Esbensen, J. U. Andersen, and H. E. Schiøtt, *Radiat. Eff.* **12**, 261 (1972).
- [27] H. E. Schiøtt, E. Bonderup, J. U. Andersen, and H. Esbensen, *Atomic Collisions in Solids* (Plenum, New York, 1974), Vol. 2, p. 843.